JACS
JOURNAL OF THE AMERICAN CHEMICAL SOCIETY
pubs.acs.org/JACS
Article

Electron-Binding Dynamics of the Dipole-Bound State: Correlation Effect on the Autodetachment Dynamics

Do Hyung Kang,† Kwang Hyun Cho,† Jinwoo Kim, Han Jun Eun, Young Min Rhee,* and Sang Kyu Kim*

Cite This: J. Am. Chem. Soc. 2023, 145, 25824−25833
Read Online
ACCESS | Metrics & More | Article Recommendations | Supporting Information

ABSTRACT: The nature of the electron-binding forces in the dipole-bound states (DBS) of anions is interrogated through experimental and theoretical means by investigating the autodetachment dynamics from DBS Feshbach resonances of *ortho*-, *meta*-, and *para*-bromophenoxide ($BrPhO^-$). Though the charge-dipole electrostatic potential has been widely regarded to be mainly responsible for the electron binding in DBS, the effect of nonclassical electron correlation has been conceived to be quite significant in terms of its static and/or dynamic contributions toward the binding of the excess electron to the neutral core. State-specific real-time autodetachment dynamics observed by picosecond time-resolved photoelectron velocity-map imaging spectroscopy reveal that the autodetachment processes from the DBS Feshbach resonances of $BrPhO^-$ anions cannot indeed be rationalized by the conventional charge-dipole potential. Specifically, the autodetachment lifetime is drastically lengthened depending on differently positioned Br-substitution, and this rate change cannot be explained within the framework of Fermi's golden rule based on the charge-dipole assumption. High-level *ab initio* quantum chemical calculations with EOM-EA-CCSD, which intrinsically takes into account electron correlations, generate more reasonable predictions on the binding energies than density functional theory (DFT) calculations, and semiclassical quantum dynamics simulations based on the EOM-EA-CCSD data excellently predict the trend in the autodetachment rates. These findings illustrate that static and dynamic properties of the excess electron in the DBS are strongly influenced by correlation interactions among electrons in the nonvalence orbital of the dipole-bound electron and highly polarizable valence orbitals of the bromine atom, which, in turn, dictate the interesting chemical fate of exotic anion species.

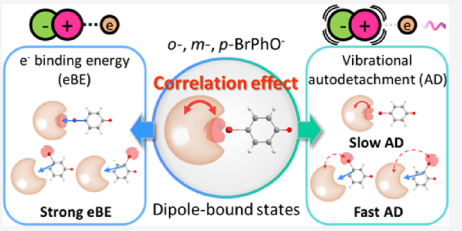

INTRODUCTION

The dipole-bound state (DBS), wherein an excess electron is loosely bound to the neutral core through the long-range monopole-dipole potential, has received keen interest in the anion physics and chemistry for many recent decades.[1−5] According to the initial conception by Fermi and Teller in 1947,[6] the minimum dipole moment for binding the excess electron in the dipole-field was predicted to be 1.625 D, which was later refined to be 2.0 D within the Born−Oppenheimer approximation.[7] As a rule of thumb, it seems to be now widely accepted that the DBS will be present if the dipole moment of the neutral core exceeds ∼2.5 D,[8,9] although some exceptional cases have recently been reported for the highly polarizable systems.[10,11] In principle, the electron-binding energy of DBS is supposed to be nearly proportional to the dipole moment of the neutral core according to the analytic expression of the pure charge-dipole interaction potential.[12] In reality, however, the electron binding energy of DBS is expected to be strongly influenced by other factors of the neutral core polarizability, induced-dipole, quadrupole, or correlation interactions.[9,13] Therefore, the classification of the nonvalence-bound state (NBS) into specific categories such as DBS, quadrupole-bound state (QBS),[14−16] or correlation-bound state (CBS)[17,18] seems to be not unambiguous as contributions of many different factors are hardly distinguishable. Despite many experimental and theoretical studies in recent years, however, the nature of the electron-binding force in the DBS beyond the charge-dipole electrostatic potential still remains elusive. For example, Gutowski et al. have reported from their *ab initio* calculations that quantum-mechanical correlation interaction should contribute significantly to the electron binding energy of the DBS even when the dipole moment (of the neutral core) exceeds 2.5 D,[19−21] although its extent could vary for different chemical systems. Furthermore, it is nontrivial to distinguish between the contribution of the charge-dipole interaction and that of the correlation interaction from the experimentally measured electron binding energy. On the other hand, it is quite notable that the electron-binding nature could be unraveled by investigation of the autodetachment dynamics

Received: September 14, 2023
Revised: October 31, 2023
Accepted: November 1, 2023
Published: November 16, 2023

https://doi.org/10.1021/jacs.3c10099
J. Am. Chem. Soc. 2023, 145, 25824−25833

at DBS Feshbach resonances where the excess electron is liberated by the vibrational motion of the neutral core as the autodetachment dynamics reflects the nature of the interaction between the charge and the neutral core.[22,23]

A recent real-time study of the picosecond time-resolved photoelectron imaging spectroscopy on the DBS autodetachment dynamics for the cryogenically cooled phenoxide anion has revealed that the autodetachment is strongly dependent on the vibrational mode characteristics.[24,25] Remarkably, Fermi's golden rule based on the charge-dipole interaction potential has been found to be extremely useful in reproducing the experiment in terms of the mode-dependent autodetachment rate for most Franck−Condon active modes, indicating that the electron-binding nature of the DBS of phenoxide could indeed be mainly attributed to the charge-dipole interaction potential. On the other hand, it has been recently found that the DBS autodetachment of the *para*-chloro or *para*-bromophenoxide anion, where the electron-rich halogen atom is situated at the same side as the electron in the diffuse nonvalence orbital, is exceptionally slow with some particular vibrational modes. This could not be rationalized by the Fermi's golden rule only with the same electrostatic charge-dipole potential.[26] Namely, the derivative of the dipole strength with respect to the normal mode displacement may not play the major role in the electron liberation in the DBS. Although the modification of the electrostatic potential that takes into account the induced-dipole by the intramolecular electric field could partially explain the qualitative trend of the experiment, the effect of the quantum-mechanical correlation interaction on the autodetachment dynamics has not yet been fully considered yet. It should be emphasized that the electron-binding nature of DBS is also closely associated with the nonadiabatic transition where the electron in the diffuse nonvalence-orbital is transferred into the valence orbital of the anion, which could lead to the eventual anionic fragmentation reactions.[27−29] As the DBS plays an important doorway role in such nonadiabatic transitions between the nonvalence- and valence-orbitals of the anion,[30−34] fundamentally understanding the relation between the nuclear motion and the electron movement (autodetachment and/or electron-transfer) of the DBS is essential for elucidating and/or controlling the whole anionic reaction dynamics.

In this context, a quantum-mechanical description of the electron-binding nature of the DBS beyond the charge-dipole potential is certainly required for a deeper understanding of the dynamic behavior of the metastable DBS, which may play important roles in many chemical and biological anionic reactions. Herein, we report combined efforts of experiment and computation to gain such insights into the autodetachment dynamics of the DBS. The mode-specific autodetachment rates at DBS Feshbach resonances of the cryogenically cooled *ortho*-, *meta*-, or *para*-bromophenoxide anions (*o*-, *m*-, or *p*-BrPhO$^-$) have been precisely measured using the picosecond time-resolved photoelectron spectroscopy. High-level *ab initio* quantum chemical calculations and semiclassical quantum dynamic simulations have additionally been carried out to reveal the quantum-mechanical effects associated with the correlation interactions along the autodetachment process. Indeed, the otherwise unexplainable large differences in the autodetachment dynamics of the DBS of the three species can be quite well rationalized by our calculations, indicating that the correlation interaction beyond the classical electrostatic charge-dipole potential should also be invoked for thoroughly understanding the electron-binding nature of the DBS. This work thus provides a new platform for properly handling the dynamics of excess electrons residing in diffuse nonvalence orbitals of anion systems.

RESULTS AND DISCUSSION

The electron affinity (EA) of each bromophenoxide isomer was precisely measured from the highest electron binding energy band of the nanosecond photoelectron spectrum, giving the results of 21 136 ± 17, 21 545 ± 32, and 20 554 ± 25 cm^{-1} for *o*-, *m*-, and *p*-BrPhO$^-$, respectively (Figure S1). EA of *p*-BrPhO$^-$ is in excellent agreement with the previously reported value of 20 551 cm^{-1} obtained from a high-resolution spectroscopic study by the Wang group.[8] It is interesting to note that the EA increases in the order of *p*-, *o*-, and *m*-BrPhO$^-$, which can be attributed to the π-donation property of the halogen-substituted on the phenyl ring that destabilizes the overall anionic resonance structure especially with the *ortho*- and the *para*-substitutions. On the other hand, the inductive effect of the electronegative bromine atom contributing to the stabilization of the anion is more significant in the *ortho*-position compared to that in the *para*-position, explaining why the EA of the former is higher than that of the latter. Similar trends had been previously reported in the studies of halogen-substituted benzyl anions[35] or iodophenoxide anions.[27] Nonresonant photoelectron spectra of the three isomers exhibit pronounced vibrational progressions of the ∼539, 523, and 295 cm^{-1} band for *o*-, *m*-, and *p*-BrPhO$^-$, respectively. According to the Franck−Condon overlap integrals in the S_0-D_0 transition, the normal mode mainly consisting of C−O in-plane stretching, which is denoted as ν_{18} (*o*- and *m*-BrPhO$^-$) or ν_{11} (*p*-BrPhO$^-$), should be responsible for the vibrational progression bands observed. It is notable that the frequency of ν_{11} of *p*-BrPhO$^-$ is much lower than the ν_{18} frequencies of *o*- and *m*-BrPhO$^-$, and this should be due to the larger effective reduced-mass of *p*-BrPhO$^-$.

The photodetachment spectrum where the photoelectron yield is taken as a function of the excitation energy was obtained for each cryogenically cooled bromophenoxide anion isomer (Figure 1). All photodetachment spectra exhibit broad background features due to direct excitations into the deionization continuum, showing monotonic increases according to Wigner's threshold law ($\sigma_{\text{detachment}} \propto \sqrt{\text{eKE}}$). There are also some notable stepwise increases arising from the cumulative openings of the quantum states leading to the deionization (Figure S2). A number of sharp bands above the broad background represent the vibrational Feshbach resonances of the DBS of each species. As the vibrational structure of the DBS should be a little different from that of the neutral species, vibrational mode assignments of the Feshbach resonances in the photodetachment spectra could be achieved quite straightforwardly from the comparison with associated vibrationally resolved bands of the photoelectron spectra. The zero-point-level (ZPL) of the DBS could be well identified in the photodetachment spectrum of each isomer as it stands out by the resonant two-photon absorption process. The DBS electron-binding energies are then estimated to be 202 ± 15, 103 ± 12, and 24 ± 12 cm^{-1} for *o*-, *m*-, and *p*-BrPhO$^-$, whose dipole moments are 4.34, 3.36, and 2.92 D, respectively. It is interesting to note that the electron-binding energy is nearly linearly proportional to the dipole size with the three isomers, giving a straight correlation line between the binding energy

https://doi.org/10.1021/jacs.3c10099
J. Am. Chem. Soc. 2023, 145, 25824−25833

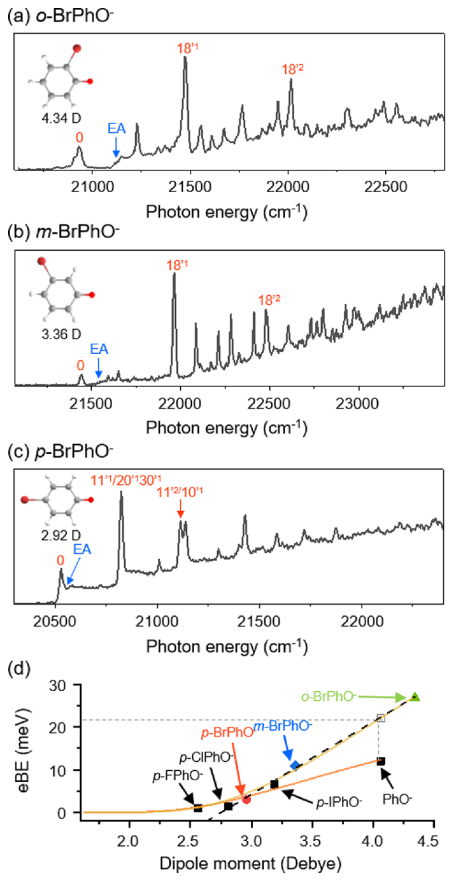

Figure 1. Nanosecond (5 ns, $\Delta E \sim 5$ cm^{-1}) photodetachment spectrum of (a) *ortho*-, (b) *meta*-, and (c) *para*-bromophenoxide anions (*o*-, *m*-, and *p*-BrPhO$^-$). The electron affinity (EA) of each anion is denoted in blue. The fundamentals and overtones of the most Franck−Condon (FC) active C−O in-plane stretching vibrational mode of the dipole-bound state (DBS) are labeled in red (see the text). Below the EA, the DBS zero-point level (0) is labeled for each isomer. The molecular structure of the neutral core of each isomer and its dipole moment are depicted in the insets. (d) DBS electron binding energy (eBE) plot with respect to the neutral core dipole moment. The analytical expression based on the point dipole model (yellow solid line) reported by Jordan et al.(ref 12, or a linear function (black dotted line) were used for fitting with the three isomers. The binding energies of the bare phenoxide (PhO$^-$) and *p*-halogen substituted phenoxide series (*p*-XPhO$^-$, X = F, Cl, or I) were also fitted with the analytical function (orange solid line), which gives roughly half of the effective point dipole charge ($q = 0.242$) compared to that from the fit based on the three bromophenoxide isomers ($q = 0.563$). See the details in the Supporting Information. The empty gray square at 4.05 D on the nonlinear fit denotes the eBE of PhO$^-$ DBS anticipated by the point dipole model, whereas the experimental values are denoted with filled black squares. The dipole moments for the three isomers were calculated using the Gaussian 09 package at the B3LYP/6-311++G(3df,3pd) level of theory.

and the dipole moment, and also giving an extrapolated threshold value of ∼2.75 D. In Figure 1d, a pseudopotential based on the point dipole model[12] was employed to give a fit to our experimental results (see details in the Supporting Information (SI)). In this figure, compared to the fitting for bare phenoxide and *p*-halogen-substituted phenoxide anions (*p*-XPhO$^-$, X = F, Cl, or I), the fitting for the three bromophenoxide isomers exhibits noticeably steeper lines. As a result, the fit parameter *q*, which corresponds to the effective charge of the point dipole, turned out to be twice larger for the three bromophenoxide isomers ($q = 0.563$) than that from the fitting for bare phenoxide and *p*-XPhO$^-$ series ($q = 0.242$). As this latter *q* value matches well with the one from the finite fixed dipole model ($q = 0.25$), such a large *q* value for the BrPhO$^-$ isomers clearly shows that their physics deviates strongly from the rather simple point dipole behavior. This implies that additional electron-neutral interactions will be needed to reproduce the electron binding energies of the three BrPhO$^-$ isomers. Also, according to the fit for BrPhO$^-$ anions, the electron-binding energy of the phenoxide DBS ($\mu \sim 4.05$ D) is expected to be ∼170 cm^{-1}, which is roughly twice larger than the experimentally observed value of ∼97 cm^{-1}.[36,37] This discrepancy again evidenced that the electron-binding of the DBS is substantially stronger with bromophenoxides in comparison with bare phenoxide, and it strongly suggests that the correlation-interaction contribution to the electron-binding force that adds to the more conventional charge-dipole interaction is much more significant for bromophenoxides than for phenoxide.

Photoelectron spectra taken at individual vibrational Feshbach resonances (Figures S3−S5) show that the vibrational propensity rule of $\Delta\nu = -1$ in the autodetachment process is rather strictly followed.[38,39] Accordingly, the photoelectron bands from the autodetachment of the various overtone ($\nu^n \rightarrow \nu^{n-1}$) or combinational band ($\nu^n\nu'^m \rightarrow \nu^{n-1}\nu'^m$ or $\nu^n\nu'^{m-1}$) could be also well identified in the photoelectron spectra, giving the appropriate mode assignments for most of DBS vibrational bands.[22,36] Similar to the features of the photoelectron spectra taken at nonresonant wavelengths, fundamental, overtone, and/or combination bands of the normal mode mainly consisting of the C−O bond stretching are found to be quite active in the photodetachment spectra (*vide supra*), and thus the fundamental and the overtone bands of ν_{18} stand out for *o*- or *m*-BrPhO$^-$ whereas ν_{11} and its combination bands are well identified for *p*-BrPhO$^-$ (Figure 1).

Picosecond time-resolved photoelectron imaging was employed for the autodetachment lifetime measurements. In order to get the transient, the picosecond pump laser pulse ($\Delta t \sim 1.7$ ps, $\Delta E \sim 20$ cm^{-1}) was tuned and fixed at the specific DBS vibrational state whereas the time-delayed picosecond probe laser pulse ($\lambda \sim 791$ nm) was given to depopulate the DBS state prepared by the pump laser pulse. By monitoring the photoelectron yield in the low-kinetic energy (LKE) or high-kinetic energy (HKE) region as a function of the pump−probe delay time, the autodetachment dynamics of individual vibrational states of the DBS could be unraveled as the autodetaching process is manifested as the sharp depletion (or increase) at the zero-delay time followed by the slower recovery (or decay) of the photoelectron signal in the LKE (or HKE) region (Figures 2 and 3). The $18'^1$ mode transient of the *o*-BrPhO$^-$ DBS gave the autodetachment lifetime (τ) of ∼14.1 ± 0.9 (HKE) or 17.3 ± 2.4 ps (LKE), and the two values are consistent with each other within the uncertainties. Autodetachment lifetime of the $18'^1$ mode of the *m*-BrPhO$^-$ DBS was found to be slightly longer at $\tau \sim 23.2 \pm 1.7$ (HKE) or 30.6 ± 5.0 ps (LKE). In contrast, the $11'^1/20'^130'^1$ ($11'^1/20'^3$) band transient of the *p*-BrPhO$^-$ DBS displayed a biexponential behavior. The corresponding photoelectron spectrum gives clear evidence of the distinct $-\nu_{11}$ or $-\nu_{20}$ ($-\nu_{30}/-2\nu_{20}$) transition due to the autodetachment from the $11'^1$ or the $20'^130'^1$ ($20'^3$) mode, respectively (Figure S5), whereas it should be emphasized that the $11'^1$ mode is most strongly

https://doi.org/10.1021/jacs.3c10099
J. Am. Chem. Soc. 2023, 145, 25824−25833

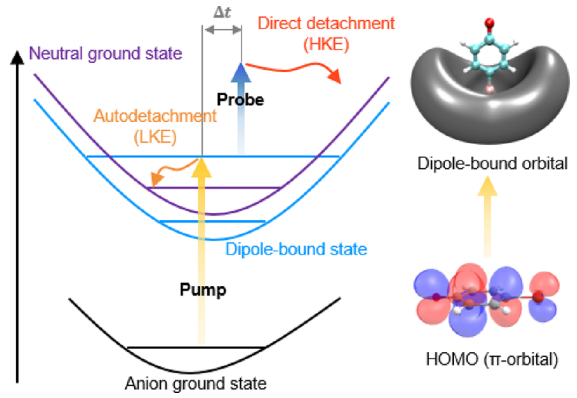

Figure 2. Schematic description of the picosecond time-resolved photoelectron imaging experiment. Pump laser pulse populates the specific vibrational states of DBS whereas the temporally delayed probe pulse depopulates those into the direct detachment continuum. The photoelectron signals in the low-kinetic energy (LKE) or high-kinetic energy (HKE) region are monitored separately, giving the real-time dynamics of the autodetached electron or the DBS-population, respectively. The schematics regarding the transition from the valence orbital of the anion to the nonvalence orbital of the DBS are also depicted.

active according to the Franck−Condon overlap. Using the picosecond time-resolved photoelectron images in the LKE region, the transients due to autodetachments of the $-\nu_{11}$ and the $-\nu_{20}$ transitions could be separately obtained with $\tau \sim 673 \pm 192$ $(-\nu_{11})$ and 71 ± 40 $(-\nu_{20})$ ps, respectively. These are quite consistent with the autodetachment lifetimes of $\tau \sim 848 \pm 127$ $(-\nu_{11})$ and 70 ± 52 $(-\nu_{20})$ ps obtained by the biexponential fit to the transient of the photoelectron in the HKE region.[26] It is quite remarkable that the autodetachment rate of the $11'^1$ DBS mode of *p*-BrPhO$^-$ is exceptionally slower compared to that of the $18'^1$ DBS mode of *o*-BrPhO$^-$ or *m*-BrPhO$^-$ by more than ∼60 times.

What is more interesting is the fact that Fermi's golden rule based on the charge-dipole potential cannot rationalize this remarkable rate difference. According to Fermi's golden rule, the autodetachment rate of the specific DBS vibrational mode (Q) is supposed to be proportional to $|\partial U/\partial Q|^2$ with electron-binding potential (U). Also, if the charge-dipole interaction potential is solely responsible for the electron-binding force, $|\partial U/\partial Q|^2$ would be directly correlated with the infrared (IR) intensity of the neutral core.[40−42] This does not appear to be the case for the DBS of *o*-, *m*-, or *p*-BrPhO$^-$ (Figure 3) as the IR intensity of the ν_{18} mode in *o*- or *m*-BrPhO· is calculated to be only two or three times larger than that of the ν_{11} mode in *p*-BrPhO·. Namely, the exceptionally slow autodetachment rate found with *p*-BrPhO$^-$ compared to that with *o*- and *m*-BrPhO$^-$ cannot be rationalized by the electrostatic charge-dipole interaction potential. As a matter of fact, a simple but improved model of the effective dipole-moment as the vector

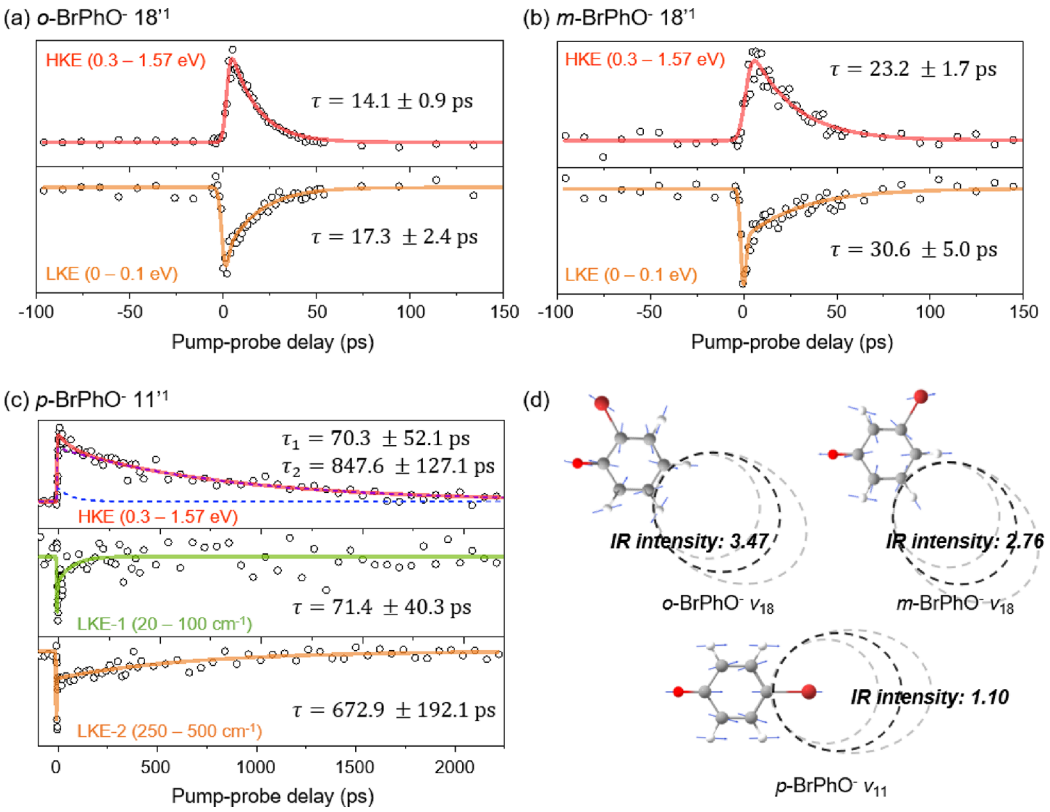

Figure 3. Picosecond time-resolved photoelectron transients for the DBSs of three bromophenoxide isomers. The photoelectron transients for the DBS vibrational modes of (a) $18'^1$ (*o*-BrPhO$^-$), (b) $18'^1$ (*m*-BrPhO$^-$), and (c) $11'^1$ (*p*- BrPhO$^-$) obtained in the HKE (red) or the LKE (green and orange) region are shown. All the transients are fit by single-exponential decay functions convoluted with a instrumental Gaussian function except for the HKE transient of *p*- BrPhO$^-$, for which a bi-exponential fit with two distinctive time constants (blue or purple dashed lines) was more adequate. (d) Schematic description of the C−O in-plane stretching modes of the *o*-, *m*-, and *p*-BrPhO· radicals. The wobbling of dipole-bound orbitals upon the molecular vibrations is sketched in black (equilibrium) or gray (at classical turning points) dashed lines according to the change of the molecular dipole moment vector. The IR intensities of the modes (in arbitrary units) are also shown.

https://doi.org/10.1021/jacs.3c10099
J. Am. Chem. Soc. 2023, 145, 25824−25833

sum of static and induced dipoles has been conceived so that the additional electrostatic potentials arising from the highly polarizable halogen moiety located near the excess electron can be incorporated into Fermi's golden rule.[26] While this improved model could successfully explain the experimentally observed trend in the earlier work, it cannot explain the rate difference found with *p*-BrPhO$^-$. This is because there are few differences in the polarizabilities of the radical species. Namely, the isotropic polarizabilities (α_{iso}) for *o*-, *m*-, and *p*-BrPhO· considered in this work were calculated to be more or less the same as 99.18, 98.55, and 102.52 Bohr^3 respectively, and the added polarized electric dipoles will likely be close to each other. We should, however, note that the position of the electron-rich bromine moiety with respect to the excess electron is very different depending on the isomer. Specifically, the excess electron is located at the positive end of the dipole (Figure 3) and its relative location with respect to the bromine atom varies much with the DBS species of *o*-, *m*-, or *p*-BrPhO$^-$. This can affect the interaction between the diffuse excess electron and the valence electrons in Br, subsequently altering the binding and detaching dynamics of the excess electron. Moreover, if the nature of the electron−electron interaction is not Coulombic but more sophisticated electron−electron correlation, a mean-field approach such as density functional theory (DFT) will not be able to capture it properly. Several attempts with DFT have indeed been made for calculating the DBS electron binding energies with augmented diffuse basis functions to handle the diffuse nature of the DBS,[43,44] and we also tried using TDDFT here. However, it failed to reproduce the electron-binding energies, which is not surprising as DFT tends to have an issue in handling long-range interactions[1,45] particularly for highly polarizable molecules with strong nondipolar interactions.[10,46] Thus, we have further carried wave function-based correlation calculations by adopting a series of different levels for comparison.[47] Interestingly, all of the methods that we tried were in good agreement with each other and correctly predicted the relative order from each species found with experiments. The results are schematically provided in Figure S7, and it indeed shows that the data from coupled-cluster based methods correspond almost excellently with the experimental ones. Certainly, we can see that we need a fairly high-level correlation approach, even for a qualitatively correct description of this type of chemistry. Hereafter, for our discussion, we will use the results from the highest level of theory, EOM-EA-CCSD.

In order to investigate the influence of the electron correlation on the binding potential, we examined the variations of the DBS binding energies for each isomer along the C−O stretching normal mode. As depicted in Figure 4, the slope of the binding energy change along this stretching mode is noticeably smaller for *p*-BrPhO· (Figure 4a). Strikingly, compared to the calculated dipole-moment changes over C−O stretching (Figure 4b), the changes in the binding energies exhibit more pronounced differences. This aspect signifies that the electron binding is dictated not only by the dipole moment but also by electron correlation. Also remarkably, the order of *p*-, *m*-, and *o*-BrPhO$^-$ with increasing changes in the binding energy is consistent with the order in the measured autodetachment rates (Figure 3). Considering that the autodetachment rate is highly dependent on the derivative of the electron-binding energy with respect to the normal mode displacement ($\partial U/\partial Q$), this finding clearly indicates that the electron correlation effect plays a significant role in the DBS

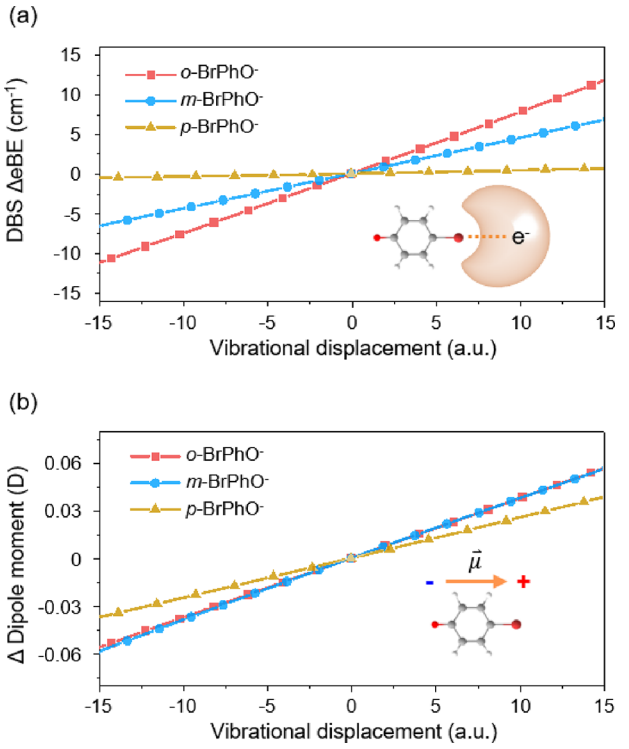

Figure 4. Changes of (a) the DBS binding energies and (b) the dipole moment of the neutral core along the C—O in-plane stretching normal mode (ν_{18} for *o*- and *m*-BrPhO$^-$, and ν_{11} for *p*-BrPhO$^-$) displacements for the three bromophenoxide anions.

autodetachment dynamics in addition to the Coulombic dipole-monopole interaction. Interestingly, the contribution by the electron correlation from *p*-BrPhO· has a mitigating effect on the contribution by the Coulombic interaction. Namely, a potential change resulting from a wobbling motion of the dipole-bound electron becomes smaller with the electron correlation than with only the dipole-monopole interaction.

While the above view on the energetics presents an insight into the interesting role of electron correlation with DBS, understanding how the autodetachment rate changes requires a consideration from the perspective of dynamics. By nature, an autodetachment process is a nonadiabatic event, and how sensitively the DBS binding energy changes upon a vibrational mode excitation, namely, the mode-specific vibronic coupling, will be a key determinant of the transition rate.[48,49] Indeed, the role of vibronic coupling in modulating nonadiabatic transitions has been extensively discussed in various systems using different computational approaches.[50−52] To investigate the impact of vibronic coupling on our autodetachment process, particularly with respect to the C−O stretching vibration, we have conducted semiclassical quantum dynamics simulations using the non-Hamiltonian variant of the Poisson bracket mapping equation (PBME-nH) formalism[53−56] after forming a minimal model Hamiltonian based on the information in Figure 4. Details of the model construction can be found in the Methods section and in the SI. The nonadiabatic transition profiles for the three isomers calculated over time, starting from their initially bound states, are depicted in Figure 5a. The simulation results are consistent with the experimentally observed order of autodetachment rates for the three isomers. By extrapolating the population

https://doi.org/10.1021/jacs.3c10099
J. Am. Chem. Soc. 2023, 145, 25824−25833

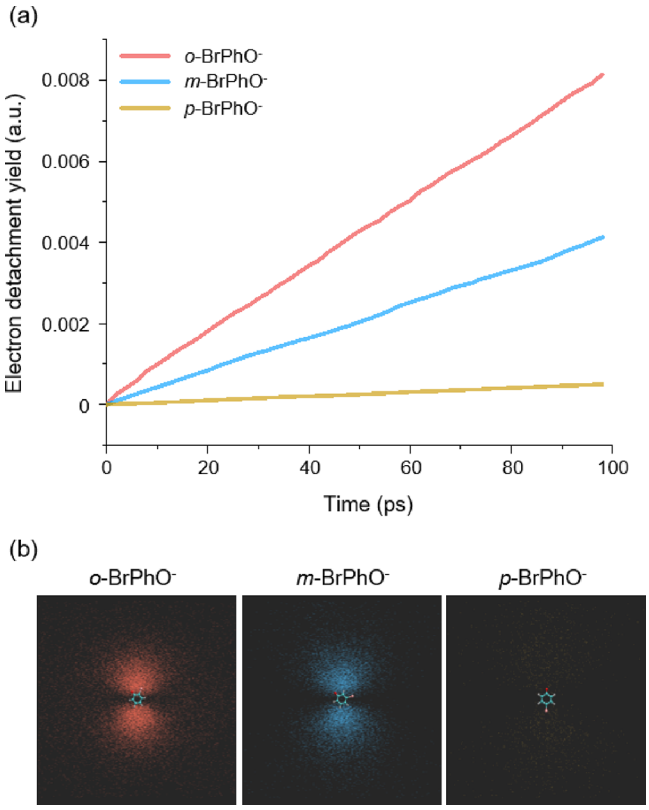

Figure 5. (a) Population of free electron detached from the DBS of each bromophenoxide anion (red: *o*-BrPhO$^-$, blue: *m*-BrPhO$^-$ and yellow: *p*-BrPhO$^-$) calculated by semiclassical quantum dynamic simulation (see details in the Supporting Information). (b) Probability distribution of the detached electrons after 100 ps from the excitation for (left) *o*-, (middle) *m*-, and (right) *p*-BrPhO$^-$ DBS.

growths of the electron-detached states, we could estimate the autodetachment lifetimes: 12.1 ns for *o*-BrPhO$^-$, 14.7 ns for *m*-BrPhO$^-$, and 207.9 ns for *p*-BrPhO$^-$. We can see that the exceptionally slow autodetachment from *p*-BrPhO$^-$ has been correctly captured with more than a 10-fold increase in the lifetime, demonstrating that an insensitive change of the interaction potential (or small vibronic coupling) leads to a deceleration of the electron detachment. In addition, although a quantitative agreement between experiment and theory for any given isomer was not reached likely due to the excessive simplicity of our minimal Hamiltonian, the trends over different isomers agree nearly excellently. We further examined the spatial distributions of the detached electron and visualized them in Figure 5b by depicting the probability distributions of the detached electron at 100 ps. Once again, slow detachment from *p*-BrPhO$^-$ is evident. With all isomers, the detached electrons exhibit distributions resembling a *p*-orbital. This shape was consistently found, even when *s*- or *d*-functions were additionally utilized for accommodating the detached electrons. This observation reflects the selection rule that arises from angular momentum conservation associated with the photoelectron effect, where the angular momentum is transferred from the neutral core wave function to the outgoing electron with $\Delta l = \pm 1$. More specifically, because the diffuse dipole-bound orbitals take *s*-like shapes, the detached electron wave functions should follow *p*-like shapes. Overall, the semiclassical simulations give at least a qualitative explanation for the exceptionally slow detachment from *p*-BrPhO$^-$, despite consistent underestimations of the computed rates. In our model, the energy conservation is only fulfilled by redistributing the excess energy after a nonadiabatic transition into internal vibrations, while in reality the electron kinetic energy can also play a role. Consequently, the transition becomes statistically less probable, leading to much slower electron detachments during the simulations. We anticipate that exploring a way of including the kinetic energy of the free electron will be an intriguing subject in future investigations. This may be achieved by adopting basis functions that can intrinsically include kinetic energy components.[57] In any case, the nearly excellent reproduction of the trend in the transition rates of the three isomers is indeed striking.

While our combined experimental and computational efforts have provided clear evidence for the tightly linked relationship between the extent of correlation interaction and the autodetachment rate, further elucidating why the electron correlation mitigates the influence of Coulombic interaction on the dipole-bound electron will be intriguing. Toward this elucidation, we have generated the Dyson orbitals for the DBS of the three isomers. With this, we observed that there are some morphological differences, particularly with *p*-BrPhO$^-$ (Figure S6).[58] In the *o*- and *m*-species, the diffuse orbitals are located on opposite sides of the electron-rich oxygen and bromine groups surrounding the neutral core, and the orbitals end up resembling an *s*-type orbital. However, in the *para*-species, the dipole-bound orbital is more diffusely distributed in space due to the large atomic size and highly polarizable occupied orbitals of the bromine atom. This diffuse nature of the dipole-bound orbital in *p*-BrPhO$^-$ may consequently render it less susceptible to perturbations from neutral core vibrations, resulting in a slow autodetachment rate. We already ascribed the rate difference to the electron correlation affecting the diffuse dipole-bound electron and the diffuse valence electrons on the highly polarizable bromine atom. From Figure S6, we can easily imagine that this correlation effect will be the largest with *p*-BrPhO$^-$, where these two types of orbitals are facing each other in closer proximity. In fact, from the viewpoint of the one-electron orbital picture, as correlation involves electron configurations bearing occupied-to-virtual excitation(s), reasoning on its physical effect may be somewhat unstraightforward. However, we can still attempt to rationalize its effect with *p*-BrPhO$^-$ in the following manner. Due to the symmetry constraint, the virtual orbital that most strongly correlates with the dipole-bound electron orbital will be a σ-type attached on the bromine atom. Because an electron in any σ-type virtual on bromine will reduce the dipole moment of *p*-BrPhO$^-$, when a configuration that bears the orbital as occupied contributes importantly, it will compensate for the effect of the apparent dipole moment dictated without electron correlation. In addition, the correlation will also be severely affected by the overlap between the spatial extents of the dipole-bound orbital and the σ-type virtual one; this compensation will be most pronounced with *p*-BrPhO$^-$.

The strong influence of the correlation interaction on the electron binding dynamics of the DBS has significant implications in the anionic chemistry of many different situations. Strengthening the electron binding by the correlation interaction, for instance, could effectively delay ultrafast electron autodetachment, thereby potentially promoting anionic chemical reactions in atmospheric or interstellar environments. Given the anticipated influence of correlation interactions, particularly in the context of highly diffuse

https://doi.org/10.1021/jacs.3c10099
J. Am. Chem. Soc. 2023, 145, 25824−25833

polycyclic aromatic hydrocarbons (PAHs),[59] it becomes conceivable that the formation of interstellar anions possessing a dipolar neutral core assumes relevance in countering the electron correlation effect.[60,61] Furthermore, the ability to modulate autodetachment rates through chemical substitutions may also offer a new tool for anionic chemical reaction controls, which can be utilized to manipulate the yields of anion formation or its subsequent bond rupture associated with the electron attachment. Of course, such a task can also be achieved selectively in combination with site-specific substitutions within the neutral molecular core.

CONCLUSIONS

Important new aspects of the electron-binding nature of the DBS have been unraveled by the combined efforts from the experimental and theoretical perspectives on the mode-specific autodetachment dynamics of the *ortho-*, *meta-*, or *para-*bromophenoxide anions. Especially, the effects of the correlation interaction on static and dynamic behaviors of the excess electron (mainly) bound in the dipole-field of the neutral core have been proven to be quite significant. For instance, the exceptionally slow autodetachment rate found with the C−O in-plane stretching $11'^{1}$ vibrational mode excitation of *p*-$BrPhO^-$ DBS, compared with the autodetachment rates measured with the corresponding C−O in-plane stretching $18'^{1}$ modes of *o-* and *m*-$BrPhO^-$, could not be explained within the framework of Fermi's golden rule solely based on the charge-dipole interaction potential. High-level *ab initio* quantum-chemical calculations that intrinsically bear the correlation interaction, combined with the semiclassical quantum dynamic calculations, gave excellent explanations for the seemingly nonintuitive experiment on the autodetachment dynamics of three isomers of the bromophenoxide anions. It was also confirmed that the static and dynamic properties of the excess electron of the DBS are strongly influenced by the correlation interactions between valence and nonvalence electrons. Considering the growing recognition of DBS as a dynamic doorway-state in a variety of anionic chemical reactions, this work not only gives a deeper understanding of the electron-binding nature of DBS but potentially promises a novel way of dynamically controlling competitively occurring autodetachments and nonadiabatic transitions from the nonvalence to the valence orbitals.

METHODS

Experimental Methods. Details of the experimental methods had been described elsewhere.[62] Briefly, 1 mM *ortho-*, *meta-*, or *para-*bromophenol (TCI Chemicals. Inc.) was dissolved in the 9:1 methanol:water solution without any further purification. A few drops of ammonia solution were added to set the acidity of the solution to pH ∼ 9. The anions of each isomer were generated from the negative mode of the homemade electrospray ionization source by applying the emission voltage of −3 kV. Anions were guided into the cryogenically cooled (8 K) Paul ion trap (Jordan TOF Inc.) by a series of RF multipole ion guides (Ardara Technologies Inc.), and then internally cooled for ∼50 ms through collisions with the He/H_2 4:1 mixture buffer gas. The cryogenically cooled anions were extracted from the ion-trap to be accelerated into our velocity-map photoelectron imaging apparatus. Photoelectrons extracted from the anions by the interaction with the pico- or nanosecond laser pulses were detected by the chevron-type microchannel plates coupled with a P43 phosphor screen (Photonis) and a charge-coupled device (CCD) camera. Picosecond pump- or probe-laser pulses were generated from the fundamental of a picosecond Ti:sapphire regenerative amplifier (Legend Elite-P, Coherent) seeded by a femtosecond Ti:sapphire oscillator (Vitara-T-HP, Coherent). The 791 nm fundamental picosecond laser pulse was split into two halves where one was used to pump the picosecond OPA system (TOPAS-800, Light Conversion) to generate the pump laser pulse whereas the other half of the fundamental was used for the probe laser pulse. The optical delay time between the pump and probe pulses was controlled by a motorized optical linear stage (DDS220, Thorlabs) coupled with a retro-reflector (UBBR-2.5-UV, Newport). The tunable nanosecond laser pulse was generated from a Nd:YAG laser system coupled with a multiple harmonic generator (NT342, Ekspla).

Computational Methods. *Electronic Structure Calculations.* All electronic structure calculations were conducted with Q-Chem 5.4.[63] As it is well acknowledged that the morphology of the DBS potential energy surface closely resembles the neutral state one, we utilized the optimized geometries of the neutral species and their normal modes, computed at the B3LYP/aug-cc-pVDZ level of theory.[64] The same level was also employed to calculate the dipole moments. Toward calculating the DBS binding energies along the C−O stretching normal mode displacement, the equation-of-motion electron-affinity coupled cluster singles and doubles (EOM-EA-CCSD) approach[65] was adopted with the same aug-cc-pVDZ basis set, together with additional even-tempered basis functions to better describe the loosely bound electron. The potential of using a less demanding theory was also explored by computing the electron binding energies with EOM-EA-CC2[66] as well as its matches within the algebraic diagrammatic construction and the Møller−Plesset realms, namely, EA-ADC(2)[67] and EOM-EA-MP2.[68] More details can be found in the SI.

Semiclassical Quantum Dynamics (PBME-nH) Simulations. The electronic subsystem Hamiltonian was assumed to consist of two electronic states, the DBS and the electron-detached state. We included a harmonic underdamped vibration for representing the C−O stretching mode, which is coupled to the energy difference between the two states. The coupling strength was determined for each isomer based on the data presented in Figure 4. This underdamped mode thus induces nonadiabatic coupling between the two states.[57] Environmental fluctuations were also included in the form of a Debye spectral density, with a dephasing time corresponding to 5 cm^{-1} and a reorganization energy of 20 cm^{-1}. Initially, the system was prepared in the DBS and was propagated for 100 ps over 1,000 trajectories to illustrate the population transfer from the DBS to the electron-detached state. More technical details can also be found in the SI.

ASSOCIATED CONTENT

Supporting Information

The Supporting Information is available free of charge at https://pubs.acs.org/doi/10.1021/jacs.3c10099.

Details of the DBS vibrational peak assignments; resonant/nonresonant photoelectron spectra; sketches of the Dyson orbitals; and supporting details of the adopted experimental/theoretical methods (PDF)

AUTHOR INFORMATION

Corresponding Authors

Young Min Rhee − *Department of Chemistry, KAIST, Daejeon 34141, Republic of Korea;* orcid.org/0000-0002-2392-3962; Email: ymrhee@kaist.ac.kr

Sang Kyu Kim − *Department of Chemistry, KAIST, Daejeon 34141, Republic of Korea;* orcid.org/0000-0003-4803-1327; Email: sangkyukim@kaist.ac.kr

Authors

Do Hyung Kang − *Department of Chemistry, KAIST, Daejeon 34141, Republic of Korea;* Present Address: Department of

Chemistry, University of California, Berkeley, California, 94720, United States; orcid.org/0000-0003-4774-9062
Kwang Hyun Cho − *Department of Chemistry, KAIST, Daejeon 34141, Republic of Korea;* orcid.org/0000-0003-1316-3063
Jinwoo Kim − *Department of Chemistry, KAIST, Daejeon 34141, Republic of Korea;* orcid.org/0000-0003-2967-6904
Han Jun Eun − *Department of Chemistry, KAIST, Daejeon 34141, Republic of Korea;* Present Address: Gas Metrology Group, Division of Chemical Biological Metrology, Korea Research Institute of Standards and Science (KRISS), Daejeon 34113, Republic of Korea; orcid.org/0000-0002-0848-0948

Complete contact information is available at: https://pubs.acs.org/10.1021/jacs.3c10099

Author Contributions

[†]D.H.K. and K.H.C. contributed equally

Notes

The authors declare no competing financial interest.

■ ACKNOWLEDGMENTS

This work was supported by the National Research Foundation of Korea under NRF-2019-Fostering Core Leaders of the Future Basic Science Program/Global PhD Fellowship Program (K.H.C.), Mid-Career Researcher Program with Grant No. 2021R1A2C2094153 (Y.M.R.), and RS-2023-00208926 (S. K. K).

■ REFERENCES

(1) Jordan, K. D.; Wang, F. Theory of Dipole-Bound Anions. *Annu. Rev. Phys. Chem.* **2003**, *54*, 367−396.
(2) Compton, R. N.; Hammer, N. I. Multipole-bound Molecular Anions. *Advances in Gas Phase Chemistry* **2001**, *4*, 257−305.
(3) Simons, J. Molecular Anions. *J. Phys. Chem. A* **2008**, *112*, 6401−6511.
(4) Lykke, K. R.; Mead, R. D.; Lineberger, W. C. Observation of Dipole-Bound States of Negative Ions. *Phys. Rev. Lett.* **1984**, *52*, 2221−2224.
(5) Verlet, J. R. R.; Anstöter, C. S.; Bull, J. N.; Rogers, J. P. Role of Nonvalence States in the Ultrafast Dynamics of Isolated Anions. *J. Phys. Chem. A* **2020**, *124*, 3507−3519.
(6) Fermi, E.; Teller, E. The Capture of Negative Mesotrons in Matter. *Phys. Rev.* **1947**, *72*, 399−408.
(7) Garrett, W. R. Critical binding of an electron to a non-stationary electric dipole. *Chem. Phys. Lett.* **1970**, *5*, 393−397.
(8) Qian, C.-H.; Zhu, G.-Z.; Wang, L.-S. Probing the Critical Dipole Moment To Support Excited Dipole-Bound States in Valence-Bound Anions. *J. Phys. Chem. Lett.* **2019**, *10*, 6472−6477.
(9) Desfrançois, C.; Abdoul-Carime, H.; Khelifa, N.; Schermann, J. P. From 1/r to $1/r^2$ Potentials: Electron Exchange between Rydberg Atoms and Polar Molecules. *Phys. Rev. Lett.* **1994**, *73*, 2436−2439.
(10) Yuan, D.-F.; Liu, Y.; Zhang, Y.-R.; Wang, L.-S. Observation of a Polarization-Assisted Dipole-Bound State. *J. Am. Chem. Soc.* **2023**, *145*, 5512−5522.
(11) Zhang, Y.-R.; Yuan, D.-F.; Qian, C.-H.; Zhu, G.-Z.; Wang, L.-S. Role of Polarization Interactions in the Formation of Dipole-Bound States. *J. Am. Chem. Soc.* **2023**, *145*, 14952−14962.
(12) Slimak, S.; Jordan, K. D. Binding of an Electron by a Finite Fixed Dipole. *J. Phys. Chem. Lett.* **2022**, *13*, 10331−10334.
(13) Abdoul-Carime, H.; Desfrançois, C. Electrons weakly bound to molecules by dipolar, quadrupolar or polarization forces. *Eur. Phys. J. D* **1998**, *2*, 149−156.
(14) Desfrançois, C.; Bouteiller, Y.; Schermann, J. P.; Radisic, D.; Stokes, S. T.; Bowen, K. H.; Hammer, N. I.; Compton, R. N. Long-Range Electron Binding to Quadrupolar Molecules. *Phys. Rev. Lett.* **2004**, *92*, No. 083003.
(15) Zhu, G.-Z.; Liu, Y.; Wang, L.-S. Observation of Excited Quadrupole-Bound States in Cold Anions. *Phys. Rev. Lett.* **2017**, *119*, No. 023002.
(16) Sommerfeld, T.; Dreux, K. M.; Joshi, R. Excess Electrons Bound to Molecular Systems with a Vanishing Dipole but Large Molecular Quadrupole. *J. Phys. Chem. A* **2014**, *118*, 7320−7329.
(17) Voora, V. K.; Cederbaum, L. S.; Jordan, K. D. Existence of a Correlation Bound s-Type Anion State of C_{60}. *J. Phys. Chem. Lett.* **2013**, *4*, 849−853.
(18) Bull, J. N.; Verlet, J. R. R. Observation and ultrafast dynamics of a nonvalence correlation-bound state of an anion. *Sci. Adv.* **2017**, *3*, No. e1603106.
(19) Gutowski, M.; Jordan, K. D.; Skurski, P. Electronic Structure of Dipole-Bound Anions. *J. Phys. Chem. A* **1998**, *102*, 2624−2633.
(20) Gutowski, M.; Skurski, P. Dispersion Stabilization of Solvated Electrons and Dipole-Bound Anions. *J. Phys. Chem. B* **1997**, *101*, 9143−9146.
(21) Gutowski, M.; Skurski, P.; Boldyrev, A. I.; Simons, J.; Jordan, K. D. Contribution of electron correlation to the stability of dipole-bound anionic states. *Phys. Rev. A* **1996**, *54*, 1906−1909.
(22) Zhu, G.-Z.; Wang, L.-S. High-resolution photoelectron imaging and resonant photoelectron spectroscopy via noncovalently bound excited states of cryogenically cooled anions. *Chem. Sci.* **2019**, *10*, 9409−9423.
(23) Kang, D. H.; Kim, J.; Noh, H.-R.; Kim, S. K. Observation of the ponderomotive effect in non-valence bound states of polyatomic molecular anions. *Nat. Commun.* **2021**, *12*, 7098.
(24) Kang, D. H.; An, S.; Kim, S. K. Real-Time Autodetachment Dynamics of Vibrational Feshbach Resonances in a Dipole-Bound State. *Phys. Rev. Lett.* **2020**, *125*, No. 093001.
(25) Kang, D. H.; Kim, J.; Eun, H. J.; Kim, S. K. State-Specific Chemical Dynamics of the Nonvalence Bound State of the Molecular Anions. *Acc. Chem. Res.* **2022**, *55*, 3032−3042.
(26) Kang, D. H.; Kim, J.; Kim, S. K. Dynamic role of the correlation effect revealed in the exceptionally slow autodetachment rates of the vibrational Feshbach resonances in the dipole-bound state. *Chem. Sci.* **2022**, *13*, 2714−2720.
(27) Kang, D. H.; Kim, J.; Eun, H. J.; Kim, S. K. Experimental Observation of the Resonant Doorways to Anion Chemistry: Dynamic Role of Dipole-Bound Feshbach Resonances in Dissociative Electron Attachment. *J. Am. Chem. Soc.* **2022**, *144*, 16077−16085.
(28) Kang, D. H.; Kim, J.; Kim, S. K. Recapture of the Nonvalence Excess Electron into the Excited Valence Orbital Leads to the Chemical Bond Cleavage in the Anion. *J. Phys. Chem. Lett.* **2021**, *12*, 6383−6388.
(29) Narayanan, S. J.; Tripathi, D.; Dutta, A. K. Doorway Mechanism for Electron Attachment Induced DNA Strand Breaks. *J. Phys. Chem. Lett.* **2021**, *12*, 10380−10387.
(30) Sommerfeld, T. Dipole-bound states as doorways in (dissociative) electron attachment. *J. Phys.: Conf. Ser.* **2005**, *4*, 245−250.
(31) Kunin, A.; Neumark, D. M. Time-resolved radiation chemistry: femtosecond photoelectron spectroscopy of electron attachment and photodissociation dynamics in iodide−nucleobase clusters. *Phys. Chem. Chem. Phys.* **2019**, *21*, 7239−7255.
(32) Koga, M.; Asplund, M.; Neumark, D. M. Electron attachment dynamics following UV excitation of iodide-2-thiouracil complexes. *J. Chem. Phys.* **2022**, *156*, No. 244302.
(33) Liu, G.; Ciborowski, S. M.; Graham, J. D.; Buytendyk, A. M.; Bowen, K. H. Photoelectron spectroscopic study of dipole-bound and valence-bound nitromethane anions formed by Rydberg electron transfer. *J. Chem. Phys.* **2020**, *153*, No. 044307.
(34) Narayanan, S. J.; Tripathi, D.; Verma, P.; Adhikary, A.; Dutta, A. K. Secondary Electron Attachment-Induced Radiation Damage to Genetic Materials. *ACS Omega* **2023**, *8*, 10669−10689.

(35) Kim, J. B.; Wenthold, P. G.; Lineberger, W. C. Ultraviolet Photoelectron Spectroscopy of o-, m-, and p-Halobenzyl Anions. *J. Phys. Chem. A* **1999**, *103*, 10833−10841.
(36) Liu, H.-T.; Ning, C.-G.; Huang, D.-L.; Dau, P. D.; Wang, L.-S. Observation of Mode-Specific Vibrational Autodetachment from Dipole-Bound States of Cold Anions. *Angew. Chem., Int. Ed.* **2013**, *52*, 8976−8979.
(37) Zhu, G.-Z.; Qian, C.-H.; Wang, L.-S. Dipole-bound excited states and resonant photoelectron imaging of phenoxide and thiophenoxide anions. *J. Chem. Phys.* **2018**, *149*, No. 164301.
(38) Acharya, P. K.; Kendall, R. A.; Simons, J. Vibration-induced electron detachment in molecular anions. *J. Am. Chem. Soc.* **1984**, *106*, 3402−3407.
(39) Simons, J. Propensity rules for vibration-induced electron detachment of anions. *J. Am. Chem. Soc.* **1981**, *103*, 3971−3976.
(40) Neumark, D. M.; Lykke, K. R.; Andersen, T.; Lineberger, W. C. Infrared spectrum and autodetachment dynamics of NH^-. *J. Chem. Phys.* **1985**, *83*, 4364−4373.
(41) Anstöter, C. S.; Mensa-Bonsu, G.; Nag, P.; Ranković, M.; Kumar, T. P. R.; Boichenko, A. N.; Bochenkova, A. V.; Fedor, J.; Verlet, J. R. R. Mode-Specific Vibrational Autodetachment Following Excitation of Electronic Resonances by Electrons and Photons. *Phys. Rev. Lett.* **2020**, *124*, No. 203401.
(42) Yokoyama, K.; Leach, G. W.; Kim, J. B.; Lineberger, W. C.; Boldyrev, A. I.; Gutowski, M. Autodetachment spectroscopy and dynamics of vibrationally excited dipole-bound states of H_2CCC^-. *J. Chem. Phys.* **1996**, *105*, 10706−10718.
(43) Takayanagi, T.; Asakura, T.; Motegi, H. Theoretical Study on the Mechanism of Low-Energy Dissociative Electron Attachment for Uracil. *J. Phys. Chem. A* **2009**, *113*, 4795−4801.
(44) Yuan, D.-F.; Zhang, Y.-R.; Qian, C.-H.; Liu, Y.; Wang, L.-S. Probing the Dipole-Bound State in the 9-Phenanthrolate Anion by Photodetachment Spectroscopy, Resonant Two-Photon Photoelectron Imaging, and Resonant Photoelectron Spectroscopy. *J. Phys. Chem. A* **2021**, *125*, 2967−2976.
(45) Sommerfeld, T. Multipole-bound states of succinonitrile and other dicarbonitriles. *J. Chem. Phys.* **2004**, *121*, 4097−4104.
(46) Yuan, D.-F.; Liu, Y.; Qian, C.-H.; Zhang, Y.-R.; Rubenstein, B. M.; Wang, L.-S. Observation of a π-Type Dipole-Bound State in Molecular Anions. *Phys. Rev. Lett.* **2020**, *125*, No. 073003.
(47) Skurski, P.; Gutowski, M.; Simons, J. How to choose a one-electron basis set to reliably describe a dipole-bound anion. *Int. J. Quantum Chem.* **2000**, *80*, 1024−1038.
(48) Saito, S.; Higashi, M.; Fleming, G. R. Site-Dependent Fluctuations Optimize Electronic Energy Transfer in the Fenna−Matthews−Olson Protein. *J. Phys. Chem. B* **2019**, *123*, 9762−9772.
(49) Lee, M. K.; Coker, D. F. Modeling Electronic-Nuclear Interactions for Excitation Energy Transfer Processes in Light-Harvesting Complexes. *J. Phys. Chem. Lett.* **2016**, *7*, 3171−3178.
(50) Dijkstra, A. G.; Wang, C.; Cao, J.; Fleming, G. R. Coherent Exciton Dynamics in the Presence of Underdamped Vibrations. *J. Phys. Chem. Lett.* **2015**, *6*, 627−632.
(51) Bose, A.; Makri, N. All-Mode Quantum−Classical Path Integral Simulation of Bacteriochlorophyll Dimer Exciton-Vibration Dynamics. *J. Phys. Chem. B* **2020**, *124*, 5028−5038.
(52) Bhattacharyya, P.; Fleming, G. R. Quantum Ratcheted Photophysics in Energy Transport. *J. Phys. Chem. Lett.* **2020**, *11*, 8337−8345.
(53) Kim, H. W.; Rhee, Y. M. Improving long time behavior of Poisson bracket mapping equation: A non-Hamiltonian approach. *J. Chem. Phys.* **2014**, *140*, No. 184106.
(54) Bonella, S.; Coker, D. F. Semiclassical implementation of the mapping Hamiltonian approach for nonadiabatic dynamics using focused initial distribution sampling. *J. Chem. Phys.* **2003**, *118*, 4370−4385.
(55) Kim, H.; Nassimi, A.; Kapral, R. Quantum-classical Liouville dynamics in the mapping basis. *J. Chem. Phys.* **2008**, *129*, No. 084102.
(56) Kim, I.; Cho, K. H.; Jeon, S. O.; Son, W.-J.; Kim, D.; Rhee, Y. M.; Jang, I.; Choi, H.; Kim, D. S. Three States Involving Vibronic Resonance is a Key to Enhancing Reverse Intersystem Crossing Dynamics of an Organoboron-Based Ultrapure Blue Emitter. *JACS Au* **2021**, *1*, 987−997.
(57) Issler, K.; Mitrić, R.; Petersen, J. Quantum−classical dynamics of vibration-induced autoionization in molecules. *J. Chem. Phys.* **2023**, *158*, No. 034107.
(58) Ortiz, J. V. Dyson-orbital concepts for description of electrons in molecules. *J. Chem. Phys.* **2020**, *153*, No. 070902.
(59) Voora, V. K.; Jordan, K. D. Nonvalence Correlation-Bound Anion States of Polycyclic Aromatic Hydrocarbons. *J. Phys. Chem. Lett.* **2015**, *6*, 3994−3997.
(60) Ashworth, E. K.; Anstöter, C. S.; Verlet, J. R. R.; Bull, J. N. Autodetachment dynamics of 2-naphthoxide and implications for astrophysical anion abundance. *Phys. Chem. Chem. Phys.* **2021**, *23*, 5817−5823.
(61) Qian, C.-H.; Zhang, Y.-R.; Yuan, D.-F.; Wang, L.-S. Photodetachment spectroscopy and resonant photoelectron imaging of cryogenically cooled 1-pyrenolate. *J. Chem. Phys.* **2021**, *154*, No. 094308.
(62) Kang, D. H.; Kim, J.; Cheng, M.; Kim, S. K. Mode-Specific Autodetachment Dynamics of an Excited Non-valence Quadrupole-Bound State. *J. Phys. Chem. Lett.* **2021**, *12*, 1947−1954.
(63) Epifanovsky, E.; Gilbert, A. T. B.; Feng, X.; Lee, J.; Mao, Y.; Mardirossian, N.; Pokhilko, P.; White, A. F.; Coons, M. P.; Dempwolff, A. L.; Gan, Z.; Hait, D.; Horn, P. R.; Jacobson, L. D.; Kaliman, I.; Kussmann, J.; Lange, A. W.; Lao, K. U.; Levine, D. S.; Liu, J.; McKenzie, S. C.; Morrison, A. F.; Nanda, K. D.; Plasser, F.; Rehn, D. R.; Vidal, M. L.; You, Z.-Q.; Zhu, Y.; Alam, B.; Albrecht, B. J.; Aldossary, A.; Alguire, E.; Andersen, J. H.; Athavale, V.; Barton, D.; Begam, K.; Behn, A.; Bellonzi, N.; Bernard, Y. A.; Berquist, E. J.; Burton, H. G. A.; Carreras, A.; Carter-Fenk, K.; Chakraborty, R.; Chien, A. D.; Closser, K. D.; Cofer-Shabica, V.; Dasgupta, S.; de Wergifosse, M.; Deng, J.; Diedenhofen, M.; Do, H.; Ehlert, S.; Fang, P.-T.; Fatehi, S.; Feng, Q.; Friedhoff, T.; Gayvert, J.; Ge, Q.; Gidofalvi, G.; Goldey, M.; Gomes, J.; González-Espinoza, C. E.; Gulania, S.; Gunina, A. O.; Hanson-Heine, M. W. D.; Harbach, P. H. P.; Hauser, A.; Herbst, M. F.; Hernández Vera, M.; Hodecker, M.; Holden, Z. C.; Houck, S.; Huang, X.; Hui, K.; Huynh, B. C.; Ivanov, M.; Jász, Á.; Ji, H.; Jiang, H.; Kaduk, B.; Kähler, S.; Khistyaev, K.; Kim, J.; Kis, G.; Klunzinger, P.; Koczor-Benda, Z.; Koh, J. H.; Kosenkov, D.; Koulias, L.; Kowalczyk, T.; Krauter, C. M.; Kue, K.; Kunitsa, A.; Kus, T.; Ladjánszki, I.; Landau, A.; Lawler, K. V.; Lefrancois, D.; Lehtola, S.; Li, R. R.; Li, Y.-P.; Liang, J.; Liebenthal, M.; Lin, H.-H.; Lin, Y.-S.; Liu, F.; Liu, K.-Y.; Loipersberger, M.; Luenser, A.; Manjanath, A.; Manohar, P.; Mansoor, E.; Manzer, S. F.; Mao, S.-P.; Marenich, A. V.; Markovich, T.; Mason, S.; Maurer, S. A.; McLaughlin, P. F.; Menger, M. F. S. J.; Mewes, J.-M.; Mewes, S. A.; Morgante, P.; Mullinax, J. W.; Oosterbaan, K. J.; Paran, G.; Paul, A. C.; Paul, S. K.; Pavošević, F.; Pei, Z.; Prager, S.; Proynov, E. I.; Rák, Á.; Ramos-Cordoba, E.; Rana, B.; Rask, A. E.; Rettig, A.; Richard, R. M.; Rob, F.; Rossomme, E.; Scheele, T.; Scheurer, M.; Schneider, M.; Sergueev, N.; Sharada, S. M.; Skomorowski, W.; Small, D. W.; Stein, C. J.; Su, Y.-C.; Sundstrom, E. J.; Tao, Z.; Thirman, J.; Tornai, G. J.; Tsuchimochi, T.; Tubman, N. M.; Veccham, S. P.; Vydrov, O.; Wenzel, J.; Witte, J.; Yamada, A.; Yao, K.; Yeganeh, S.; Yost, S. R.; Zech, A.; Zhang, I. Y.; Zhang, X.; Zhang, Y.; Zuev, D.; Aspuru-Guzik, A.; Bell, A. T.; Besley, N. A.; Bravaya, K. B.; Brooks, B. R.; Casanova, D.; Chai, J.-D.; Coriani, S.; Cramer, C. J.; Cserey, G.; DePrince, A. E., III; DiStasio, R. A., Jr.; Dreuw, A.; Dunietz, B. D.; Furlani, T. R.; Goddard, W. A., III; Hammes-Schiffer, S.; Head-Gordon, T.; Hehre, W. J.; Hsu, C.-P.; Jagau, T.-C.; Jung, Y.; Klamt, A.; Kong, J.; Lambrecht, D. S.; Liang, W.; Mayhall, N. J.; McCurdy, C. W.; Neaton, J. B.; Ochsenfeld, C.; Parkhill, J. A.; Peverati, R.; Rassolov, V. A.; Shao, Y.; Slipchenko, L. V.; Stauch, T.; Steele, R. P.; Subotnik, J. E.; Thom, A. J. W.; Tkatchenko, A.; Truhlar, D. G.; Van Voorhis, T.; Wesolowski, T. A.; Whaley, K. B.; Woodcock, H. L., III; Zimmerman, P. M.; Faraji, S.; Gill, P. M. W.; Head-Gordon, M.; Herbert, J. M.; Krylov, A. I. Software for the frontiers of quantum chemistry: An

overview of developments in the Q-Chem 5 package. *J. Chem. Phys.* **2021**, *155*, No. 084801.
(64) Kendall, R. A.; Dunning, T. H.; Harrison, R. J. Electron affinities of the first-row atoms revisited. Systematic basis sets and wave functions. *J. Chem. Phys.* **1992**, *96*, 6796−6806.
(65) Zuev, D.; Jagau, T.-C.; Bravaya, K. B.; Epifanovsky, E.; Shao, Y.; Sundstrom, E.; Head-Gordon, M.; Krylov, A. I. Complex absorbing potentials within EOM-CC family of methods: Theory, implementation, and benchmarks. *J. Chem. Phys.* **2014**, *141*, No. 024102.
(66) Christiansen, O.; Koch, H.; Jørgensen, P. The second-order approximate coupled cluster singles and doubles model CC2. *Chem. Phys. Lett.* **1995**, *243*, 409−418.
(67) Wormit, M.; Rehn, D. R.; Harbach, P. H. P.; Wenzel, J.; Krauter, C. M.; Epifanovsky, E.; Dreuw, A. Investigating excited electronic states using the algebraic diagrammatic construction (ADC) approach of the polarisation propagator. *Mol. Phys.* **2014**, *112*, 774−784.
(68) Stanton, J. F.; Gauss, J. Perturbative treatment of the similarity transformed Hamiltonian in equation-of-motion coupled-cluster approximations. *J. Chem. Phys.* **1995**, *103*, 1064−1076.

https://doi.org/10.1021/jacs.3c10099
J. Am. Chem. Soc. 2023, 145, 25824−25833